ROBERT KOCH INSTITUT

Originally published as:

Title:

Cryo FIB-SEM: volume imaging of cellular ultrastructure in native frozen specimens

Andreas Schertel[1#], Nicolas Snaidero[2#], Hong-Mei Han[3], Torben Ruhwedel[4], Michael Laue[5], Markus Grabenbauer[3], Wiebke Möbius[4§*]

1) Carl Zeiss Microscopy GmbH, Training, Application and Support Center (TASC), Carl-Zeiss-Straße 22, D-73447 Oberkochen, Germany

2) Cellular Neuroscience, Max Planck Institute of Experimental Medicine, Hermann-Rein-Straße 3, D-37075 Göttingen, Germany

3) Department of Systemic Cell Biology, Max-Planck-Institute of Molecular Physiology, Otto-Hahn-Straße 11, D-44227 Dortmund, Germany

4) Department of Neurogenetics, Electron Microscopy Facility, Max-Planck-Institute of Experimental Medicine, Hermann-Rein-Straße 3, D-37075 Göttingen, Germany

5) Advanced Light and Electron Microscopy, Centre for Biological Threats and Special Pathogens, Robert Koch Institute, Nordufer 20, D-13353 Berlin, Germany

§) Center for Nanoscale Microscopy and Molecular Physiology of the Brain (CNMPB), Göttingen, Germany

# equal contribution

*correspondence to:

moebius@em.mpg.de

Wiebke Möbius

Department of Neurogenetics, Electron Microscopy Facility

Max-Planck-Institute of Experimental Medicine

Hermann-Rein-Straße 3

D-37075 Göttingen, Germany

Phone: +49-551-3899736, Fax: +49-551-3899753

Abstract

Volume microscopy at high resolution is increasingly required to better understand cellular functions in the context of three-dimensional assemblies. Focused ion beam (FIB) milling for serial block face imaging in the scanning electron microscope (SEM) is an efficient and fast method to generate such volume data for 3D analysis. Here, we apply this technique at cryo-conditions to image fully hydrated frozen specimen of mouse optic nerves and *Bacillus subtilis* spores obtained by high-pressure freezing (HPF). We established imaging conditions to directly visualize the ultrastructure in the block face at −150°C by using an in-lens secondary electron (SE) detector. By serial sectioning with a focused ion beam and block face imaging of the optic nerve we obtained a volume as large as X=7.72 µm, Y=5.79 µm and Z=3.81 µm with a lateral pixel size of 7.5 nm and a slice thickness of 30 nm in Z. The intrinsic contrast of membranes was sufficient to distinguish structures like Golgi cisternae, vesicles, endoplasmic reticulum and cristae within mitochondria and allowed for a three-dimensional reconstruction of different types of mitochondria within an oligodendrocyte and an astrocytic process. Applying this technique to dormant *Bacillus subtilis* spores we obtained volumes containing numerous spores and discovered a bright signal in the core, which can not be related to any known structure so far. In summary, we describe the use of cryo FIB-SEM as a tool for direct and fast 3D cryo-imaging of large native frozen samples including tissues.

1. Introduction

Cryo transmission electron microscopy (cryo-TEM) is the only available technique to directly image native structures at nanoscale resolution (Müller *et al.*, 2008). The introduction of cryo-electron microscopy of vitreous sections (CEMOVIS) made it possible to visualize native structures in the context of the cellular environment in the frozen hydrated state (Al-Amoudi *et al.*, 2004). In contrast to conventional transmission electron microscopy (TEM), which relies on the preferential binding of contrasting agents to proteins and lipids, in cryo-electron microscopy the image is generated by the density of the biological material itself. Therefore, these data contain highly valuable direct biological information suitable for modelling of macromolecules or membrane assemblies in their native context (Al-Amoudi et al., 2007; Leforestier et al., 2012). By cryo-electron tomography (CET) (Bouchet-Marquis and Hoenger, 2011) three dimensional (3D) views of organelles and cells are generated. However, CEMOVIS as well as CET of large specimens depend on cryo-ultramicrotomy, which inevitably induces cutting artefacts such as knife marks, compression and crevasses (Al-Amoudi *et al.*, 2005). Moreover, imaging of large cells or tissue samples in 3D by CET is limited by the section thickness and requires the toilsome effort of serial cryosectioning and reconstructing serial tomograms. Improved cryo soft X-ray microscopy was established recently to image large native frozen samples by tomography (Schneider et al., 2010; Weiner et al., 2013). This method is applicable to samples of up to 10 µm thickness at a resolution in the range of 36 to 70 nm. Unfortunately, X-ray tomography is limited so far to plunge frozen or very thin high-pressure frozen samples, since methods to prepare 10 µm thick sections of vitrified tissue samples are not yet available.

Focused ion beam (FIB) milling for serial block face imaging in the scanning electron microscope (SEM) is an efficient and fast method to generate large volume data for 3D analysis in an automated fashion (Heymann et al., 2006; Knott et al., 2008). Here,

conventional resin-embedded samples are imaged by detecting the backscattered electron (BSE) signal from the block face. FIB-milling of frozen-hydrated specimen was applied without imaging the ultrastructure directly as a preparatory step for thinning samples to a suitable size for cryo-TEM or CET instead of cryosectioning (Hayles et al., 2010; Marko et al., 2007; Rigort et al., 2012; Rigort et al., 2010; Wang et al., 2012). Important contributions to high-resolution block-face imaging of frozen specimens in cryo-SEM were made by Paul Walter and colleagues showing that many subcellular structures are revealed in remarkable detail by special BSE detection after limited surface sublimation ('freeze-etching') and double-layer coating with platinum/carbon (Walther, 2008; Walther and Müller, 1999).

Our goal was to establish imaging parameters for cryo FIB-SEM that allow the visualization of frozen hydrated cellular components like vesicles, mitochondria and other membranous organelles with sufficient resolution for the 3D modelling. This approach provides a direct tool for volume imaging that does not require dehydration, heavy metal impregnation by freeze substitution and resin-embedding. Omitting these procedures is especially interesting for samples that are sensitive to dehydration artefacts or difficult to embed in resin. Here, we evaluated this method in a proof-of-principle manner with two different biological samples, both prepared by high-pressure freezing (HPF): mouse optic nerves and dormant *Bacillus subtilis* spores.

2.   Results and Discussion

The optic nerve samples were obtained from 14 days old mice at the peak of myelination of the retinal ganglion cell axons. This tissue sample is characterized by axonal profiles showing a variety of different myelination stages and myelinating oligodendrocytes with a highly active endoplasmic reticulum (ER) and Golgi complex involved in the biosynthesis and trafficking of myelin lipids and proteins. For cryo FIB-

4

SEM, optic nerves were high-pressure frozen in a slit carrier which makes it easier to orient the frozen nerve in the cryo-holder of the SEM (**Fig. 1a**). Under cryo-conditions at −150°C by using the in-lens secondary electron (SE)-detector we were able to directly visualize the ultrastructure of myelinated and non-myelinated axons as well as cell bodies (**Fig. 1b** and **1c**). Similar features could be observed by block-face imaging at room temperature in optic nerve samples which were prepared by HPF, freeze substitution including OsO_4 and uranyl acetate staining and EPON-embedding using the BSE-signal with the energy selective backscattered electron (ESB)-detector (**Fig. 1d**). Understanding the contrast formation by secondary electrons in the native frozen block face is difficult and several aspects concerning the beam/specimen interaction during imaging have to be taken into account. The in-lens detector mainly visualizes secondary electrons which are directly generated by the interaction with the primary beam at the point of focus (the so-called SE1 electrons). These electrons are emitted with low energy and therefore, differences in the local surface potential influences the number of SE1 detected, e.g. a positive surface potential will suppress emission. We observed that areas of higher water content such as cytoplasm or extracellular space show a brighter grey level in the in-lens image than lipid-rich structures such as membranes and myelin. This effect is probably due to differences in charge dissipation which cause negative (SE1-release promoting) or positive (SE1-release suppressing) surface potentials as discussed (see chapter 5 (Stokes, 2008)). Surface potentials can be also influenced by Ga^+ implantation and loss of charged milling products during FIB milling. Furthermore, prolonged electron beam irradiation causes mass loss on the frozen sample surface creating a surface texture resulting in edge brightness. This beam induced sublimation becomes obvious after repeated scanning during focussing or leaving the electron beam in one position (**Supplementary Fig 1a** and **b**). However, this irradiation induced surface modification during recording the first image of a freshly milled surface is avoided by

proper choice of imaging parameters, but will occur after prolonged imaging of the same area (**Supplementary Fig 1c and d**).

Data sets of serial images were recorded by repeated FIB-milling and block face imaging. About 127 serial images covering volume of X = 7.72 µm, Y = 5.79 µm and Z = 3.81 µm containing half the cell body of an oligodendrocyte were obtained within 3 h at a lateral image pixel size of 7.5 nm and a FIB slice thickness of 30 nm (**Fig. 2a**). For noise reduction, line averaging (N=256) and a scan speed of 100 ns dwell time was selected experimentally. In this actively myelinating cell, mitochondria with their cristae, Golgi complex and associated transport vesicles, rough endoplasmic reticulum and nuclear envelope are clearly discernible. We reconstructed the mitochondrial network within this volume by manual segmentation (**Fig. 2b** and **Video 1**), showing that a substantial fraction of the mitochondria exhibit branching and connections (**Supplementary Fig. 2**). In an adjacent typical astrocytic process, mitochondria appear as single units with a larger diameter and simpler shape and are not connected with each other.

Since the cryo FIB-SEM images were obtained from native frozen hydrated samples, we used these data for comparison with mouse optic nerve samples that were either prepared by HPF, freeze substitution (FS) and EPON embedding or by conventional processing. To evaluate any effect of dehydration on the ultrastructure, we measured the widths of the nuclear envelope profiles of 3 individual oligodendrocyte nuclei in images obtained by the three different methods (**Fig. 2c-e**). In cryo FIB-SEM as well as in TEM images of freeze substituted samples, the nuclear envelope was characterized by narrow and dilated areas with an average width of 28.15 nm ± 3.09 SD (cryo FIB-SEM) and 26.8 nm ± 2.07 SD (HPF/FS) in contrast to the completely narrow appearance in the conventionally prepared samples with an average width of 20.7 nm ± 0.09 SD (**Supplementary Fig. 3a and b**). These data confirm that HPF and FS induce far less shrinkage than conventional sample processing. Shrinkage

was described as an artefact caused by dehydration during conventional embedding (Hayat, 2000; McDonald et al., 2007). More important, the cryo FIB-SEM data serve as a native reference for the morphology after FS, in which the contrast is formed by heavy metal impregnation. The overall morphology appears unaltered by FS, indicating that freeze substituted samples indeed resemble the native frozen state at the level of organelle morphology as discussed by Studer and coworkers (Studer et al., 2008). However, at the molecular level differences between samples prepared by FS or for CEMOVIS become evident as exemplified by Al-Amoudi and coworkers (Al-Amoudi et al., 2004). Regarding sample preparation, cryo FIB-SEM compares well to CEMOVIS, since both are based on the same kind of native frozen specimens. But due to the differences in the energy of the primary electrons and the mechanism of contrast formation, cryo FIB-SEM and CEMOVIS are not similar and their limit of resolution is at different level. If devitrification occurred during surface sublimation before platinum-coating, the ice crystals are below the resolution limit and do not cause detectable changes in morphology. This is in agreement with cryo-SEM data obtained by Paul Walther using cryosectioning, sublimation at −110°C and cryo-double-layer coating (Walther, 2003). However, warming-up of vitrified samples to −90°C occurs as well during freeze-substitution without any distortion of the samples detectable by routine TEM. On the contrary, hexagonal ice formation during insufficient freezing by HPF results in severe morphological changes which are clearly visible after FS (Möbius et al., 2010) as well as in cryo FIB-SEM (data not shown).

Dormant spores of *Bacillus subtilis* were imaged by cryo FIB-SEM (**Fig. 3a**) as well as by conventional TEM (**Fig. 3c**), and by CEMOVIS (**Fig. 3d**). So far imaging of dormant spores without risking the activation of germination was impossible since conventional aldehyde fixation may induce first steps of germination or structural changes. Moreover, high-pressure freezing followed by freeze-substitution and resin

embedding of dormant spores failed, because the membrane of the spore core remains impermeable for the resin. Only by cryo FIB-SEM it was possible to collect serial images of native high-pressure frozen spores in such a quality that allowed 3D reconstruction (**Fig. 3b** and **Video 2**). The overall organisation of the spore was the same with all of the methods employed. However, TEM imaging revealed more details than the block-face imaging by SEM, which is particularly evident in the coat and core structures (**Fig. 3d**). Most striking differences could be observed within the core. Cryo-SEM imaging of the milled block face revealed a local bright SE1-signal formation being interconnected and seeming to appear like a filamentous network in the reconstructed 3D model which was never seen before by any other technique (**Fig. 3a, b** and **Video 2**). It is unlikely that this SE signal is due to ice crystal damage, because the spore core is almost dry (Setlow, 2006). Also, beam induced mass loss occurred preferentially in the coat and cortex of the spore and not in the core (**Supplementary Fig. 1c and d**). The bright signal in the core may be related to a particular local composition, underlying structure or density in the spore core, which facilitates the release of secondary electrons in contrast to the surroundings. As already mentioned above, differences in the local surface potential could explain the differences in the yield of SE1. Three structures reveal a particular bright signal: a distinct layer of the outer coat; the meshwork within the core that partially forms a rim at the presumed position of the core membrane; the cap-like structures within the coats at both poles of the spore (**Supplementary Fig. 4a and c**). Analysis of brightness-values showed similar values for the frozen water (i.e. the buffer solution) that surrounds the spore and for the cap-like structures (**Supplementary Fig 4b and d**: brightness plot). Freeze-drying removes the water around the spores and at the position of the cap-like structures (**Supplementary Fig. 4e**), indicating that the highest brightness values are obtained in areas which contain frozen bulk water. Brightness levels of the distinct outer coat layer and core structures are lower than

brightness levels of the frozen bulk water present around the spore, but significantly higher than the values from the cortex and most layers of the coat. Thus, brightness values may correlate with surface potentials influenced by the water content as well as composition and density of biopolymers. Also subtle beam induced modifications, which may be indirectly correlated to internal composition or structure within the core, cannot be ruled out. Sophisticated experiments are needed to test this hypothesis and to address the questions of contrast formation in more detail which is essential to explain the particular signals generated by cryo FIB-SEM.

To conclude, cryo FIB-SEM allows 3D imaging of native frozen samples up to 7.5 nm pixel size. This is a suitable method to analyze volumes of samples that require remaining hydrated such as biofilms, bacterial spores and also skin as described by Richter and coworkers (Richter et al., 2007). In addition, a major advantage of this method is its unprecedented speed, since imaging can start immediately after freezing without the need for further processing such as dehydration, embedding or manual sectioning. Furthermore, substantial volumes can be imaged within a few hours, which is relevant for diagnostic or clinical purposes and is virtually impossible with CEMOVIS. Moreover, large samples like nerves can be repeatedly imaged at different spots and orientations.

3.   Materials and Methods

The generation of *Bacillus subtilis* spores, high pressure freezing, freeze substitution, conventional sample processing for TEM and CEMOVIS as well as the methods used for segmentation, 3D reconstruction and quantification are described in the Supplementary Material.

3.1.   Mounting and Sputter Coating for SEM

The slit carrier containing the high pressure frozen mouse optic nerve sample or the aluminum platelets with the *Bacillus subtitlis* sample were mounted on a cryo sample holder in the preparation box of the VCT100 shuttle system (Leica Microsystems, Vienna, Austria) at LN2 temperature. By using the VCT100 shuttle the sample holder was transferred to the SCD500 sputter coater (Leica Microsystems, Vienna, Austria) at −115°C cryo-stage temperature and $4 \cdot 10^{-6}$ mbar chamber pressure. In the sputter coater the sample was heated up to −100°C for sublimation. Immediately after reaching the target temperature the sample was cooled down to −115°C. The sample was sputter coated with an eight nanometer platinum layer at 0.06 nm/s. During sputter coating an argon pressure of $2 \cdot 10^{-2}$ mbar and a current of 55 mA was measured. After coating the sample was transferred to the Auriga60 Crossbeam® system (Carl Zeiss Microscopy GmbH, Oberkochen, Germany) by using the VCT100 shuttle at a cryo-stage temperature of −140°C. Throughout the analysis the optic nerve samples were kept at −140°C. The *Bacillus subtilis* samples were analyzed at −150°C.

3.2. FIB milling and SEM imaging

Using the 30 kV:16 nA FIB probe current a coarse incision was milled directly into the surface of the high pressure frozen optic nerve sample in order to achieve a viewing channel for the SEM imaging. This notch of about 50 µm width was fine polished using the 30 kV 600 pA FIB probe current. For acquisition of the data cube a block face of about 50 µm width using the 600 pA FIB probe current and a slice thickness of 30 nm was defined. The data cube was acquired in a fully automated process. After each slice the FIB milling procedure was paused and the region of interest (ROI) on the block face was imaged using the 7.5 µm aperture in normal mode at 2.33 kV acceleration voltage and the in-lens detector. The lateral image pixel size was 7.5 nm resulting in images covering 7.72 µm width and 5.79 µm height. For

noise reduction line averaging (N=256) and a scan speed of 100 ns dwell time was chosen. The cycle time for recording an individual image was 25.2 s. The milling time for removing each slice was 35.8 s. Accordingly, about every minute an image was recorded. The final image series consisted of 127 individual slices resulting in a volume of 7.72*5.79*3.81 µm^3.

The *Bacillus subtilis* sample was milled and imaged accordingly on a block face of 38 µm width and using a slice thickness of 15 nm. The lateral image pixel size was 9 nm covering 9.20 µm width and 6.90 µm height. For noise reduction line average (N=150) and a scan speed of 100 ns dwell time was chosen. The cycle time for recording an individual image was 14.8 s. The milling time for removing each slice was 6.83 s. This means that every minute two or three images were recorded. The image series of 170 individual slices covered a volume of 9.20*6.90*2.55 µm^3.

Appendix: Supplementary Material

References

Al-Amoudi, A., D. Studer, J. Dubochet, 2005. Cutting artefacts and cutting process in vitreous sections for cryo-electron microscopy. J Struct Biol 150, 109-21.

Al-Amoudi, A., D.C. Diez, M.J. Betts, A.S. Frangakis, 2007. The molecular architecture of cadherins in native epidermal desmosomes. 0028-0836 450, 832-7.

Al-Amoudi, A., J.J. Chang, A. Leforestier, A. McDowall, L.M. Salamin, L.P. Norlen, K. Richter, N.S. Blanc, D. Studer, J. Dubochet, 2004. Cryo-electron microscopy of vitreous sections. EMBO J 23, 3583-8.

Bouchet-Marquis, C., A. Hoenger, 2011. Cryo-electron tomography on vitrified sections: a critical analysis of benefits and limitations for structural cell biology. Micron 42, 152-62.

Hayat, M.A., 2000. Principles and Techniques of Electron Microscopy, Biological Applications, fourth edition ed. Cambridge University Press, Cambridge.

Hayles, M.F., D.A. de Winter, C.T. Schneijdenberg, J.D. Meeldijk, U. Luecken, H. Persoon, J. de Water, F. de Jong, B.M. Humbel, A.J. Verkleij, 2010. The making of frozen-hydrated, vitreous lamellas from cells for cryo-electron microscopy. J Struct Biol 172, 180-90.

Heymann, J.A., M. Hayles, I. Gestmann, L.A. Giannuzzi, B. Lich, S. Subramaniam, 2006. Site-specific 3D imaging of cells and tissues with a dual beam microscope. J Struct Biol 155, 63-73.

Knott, G., H. Marchman, D. Wall, B. Lich, 2008. Serial section scanning electron microscopy of adult brain tissue using focused ion beam milling. J Neurosci 28, 2959-64.

Leforestier, A., N. Lemercier, F. Livolant, 2012. Contribution of cryoelectron microscopy of vitreous sections to the understanding of biological membrane structure. Proc Natl Acad Sci U S A 109, 8959-64.

Marko, M., C. Hsieh, R. Schalek, J. Frank, C. Mannella, 2007. Focused-ion-beam thinning of frozen-hydrated biological specimens for cryo-electron microscopy. Nat Methods 4, 215-7.

McDonald, K.L., M. Morphew, P. Verkade, T. Müller-Reichert, 2007. Recent advances in high-pressure freezing: equipment- and specimen-loading methods. Methods Mol Biol 369, 143-73.

Möbius, W., B. Cooper, W.A. Kaufmann, C. Imig, T. Ruhwedel, N. Snaidero, A.S. Saab, F. Varoqueaux, 2010. Electron microscopy of the mouse central nervous system. Methods Cell Biol 96, 475-512.

Müller, S.A., U. Aebi, A. Engel, 2008. What transmission electron microscopes can visualize now and in the future. J Struct Biol 163, 235-45.

Richter, T., S.S. Biel, M. Sattler, H. Wenck, K.P. Wittern, R. Wiesendanger, R. Wepf, 2007. Pros and cons: cryo-electron microscopic evaluation of block faces versus cryo-sections from frozen-hydrated skin specimens prepared by different techniques. J Microsc 225, 201-7.

Rigort, A., F.J. Bauerlein, E. Villa, M. Eibauer, T. Laugks, W. Baumeister, J.M. Plitzko, 2012. Focused ion beam micromachining of eukaryotic cells for cryoelectron tomography. Proc Natl Acad Sci U S A 109, 4449-54.

Rigort, A., F.J. Bauerlein, A. Leis, M. Gruska, C. Hoffmann, T. Laugks, U. Bohm, M. Eibauer, H. Gnaegi, W. Baumeister, J.M. Plitzko, 2010. Micromachining tools and correlative approaches for cellular cryo-electron tomography. J Struct Biol 172, 169-79.

Schneider, G., P. Guttmann, S. Heim, S. Rehbein, F. Mueller, K. Nagashima, J.B. Heymann, W.G. Muller, J.G. McNally, 2010. Three-dimensional cellular ultrastructure resolved by X-ray microscopy. Nat Methods 7, 985-7.

Setlow, P., 2006. Spores of Bacillus subtilis: their resistance to and killing by radiation, heat and chemicals. J Appl Microbiol 101, 514-25.

Stokes, D.J., 2008. Principles and practise of variable pressure/environmental scanning electron microscopy (VP-ESEM). John Wiley & Sons Ltd, UK.

Studer, D., B.M. Humbel, M. Chiquet, 2008. Electron microscopy of high pressure frozen samples: bridging the gap between cellular ultrastructure and atomic resolution. Histochem Cell Biol 130, 877-89.

Walther, P., 2003. Cryo-fracturing and cryo-planing for in-lens cryo-SEM, using a newly designed diamond knife. Microsc Microanal 9, 279-85.

Walther, P., 2008. High-Resolution Cryoscanning Electron Microscopy of Biological Samples, p. 245-267, in: Schatten, H, Pawley, J B, Eds.), Biological Low-Voltage Scanning Electron Microscopy, Springer, New York, pp. 245-267.

Walther, P., M. Müller, 1999. Biological ultrastructure as revealed by high resolution cryo-SEM of block faces after cryo-sectioning. J Microsc 196, 279-87.

Wang, K., K. Strunk, G. Zhao, J.L. Gray, P. Zhang, 2012. 3D structure determination of native mammalian cells using cryo-FIB and cryo-electron tomography. J Struct Biol.

Weiner, A., S. Kapishnikov, E. Shimoni, S. Cordes, P. Guttmann, G. Schneider, M. Elbaum, 2013. Vitrification of thick samples for soft X-ray cryo-tomography by high pressure freezing. J Struct Biol 181, 77-81.

Figure Legends

Figure 1: FIB-SEM of mouse optic nerve during active myelination at the age of 14 days. (**a**) Secondary electron (SE) image of the frozen nerve in a slit carrier mounted on the cryo holder. (**b**) SE image of the frozen block face created by FIB milling visualized with the in-lens detector. (**c**) Higher magnified the block face SE image of the frozen hydrated optic nerve. (**d**) Block face image of epoxy-embedded optic nerve at room temperature after HPF and FS. The image is formed by backscattered primary electrons which are detected with the ESB detector. To resemble TEM images, the contrast was inverted. Scale bars, 500 µm (**a**), 5 µm (**b**), 1 µm (**c** and **d**).

Figure 2: 3D reconstruction of the mitochondrial network within an oligodendrocyte and appearance of the nuclear envelope after different sample preparations. (**a**) SE image of an oligodendrocyte contained in the series of images which were used for segmentation and 3D modelling. Asterisks indicate myelinated axons. n, nucleus; g, Golgi complex and mitochondria (arrowheads). (**b**) 3D model of the mitochondrial network (blue) of the oligodendrocyte with the nucleus (orange) and an astrocytic process (violet). (**c**) Perinuclear space (red coloured) on nuclear profiles of oligodendrocytes in cryo FIB-SEM images of optic nerve samples, (**d**) in TEM images

of epoxy-embedded optic nerve samples after HPF and FS and (**e**) in TEM images of conventionally processed and epoxy-embedded optic nerve samples. Scale bars, 1 µm (**a**), 200 nm (**c**, **d**, **e**)

Figure 3: Morphology of *Bacillus subtilis* spores by different microscopic methods and 3D ultrastructure derived from cryo FIB-SEM. (**a**) In-lens SE-image of a frozen spore in the block face of a sample that was milled by FIB. Arrow indicates a bright structure within the coat which is also found in conventional TEM images (**b**) 3D model of the same spore after consecutive milling and imaging. Segmentation was done for the bright signal within the core (red), the bright signal within the coat at both ends of the spores (blue) and the outer layer of the coat (transparent grey). (**c**) Conventional TEM of an ultrathin section through a plastic embedded spore. co, core; ct, coat, cx, cortex; arrow: coat structure which forms a cap (blue in (b)) at both ends of the spore (**d**) CEMOVIS image of a frozen section of a spore. All preparation and imaging methods employed reveal differences, but also overlap in the ultrastructural appearance due to differences in preparation variables and image formation. However, only Cryo-FIB-SEM allowed the imaging of spores in 3D without changing the chemical environment during preparation thereby avoiding any activation or significant structural changes. Scale bars, 200 nm.

Figure 1
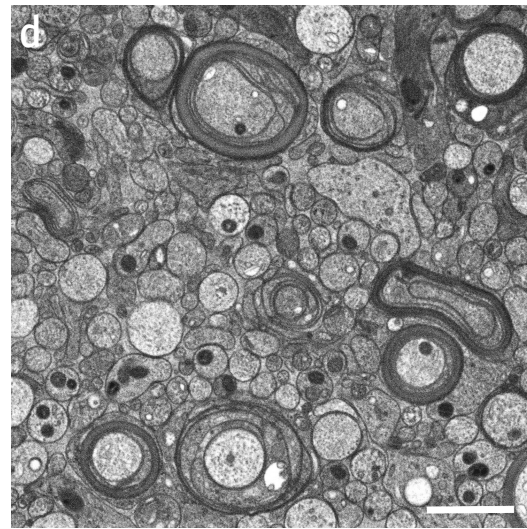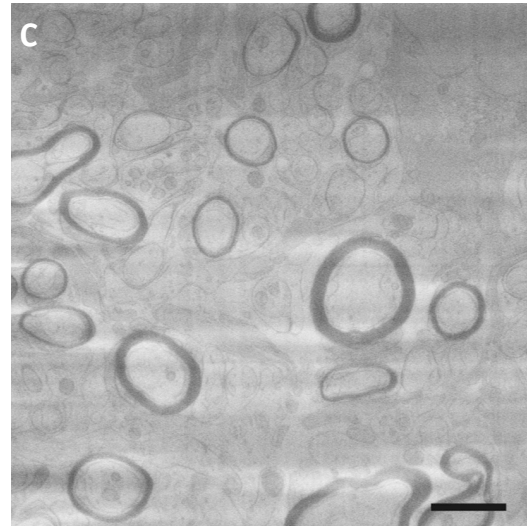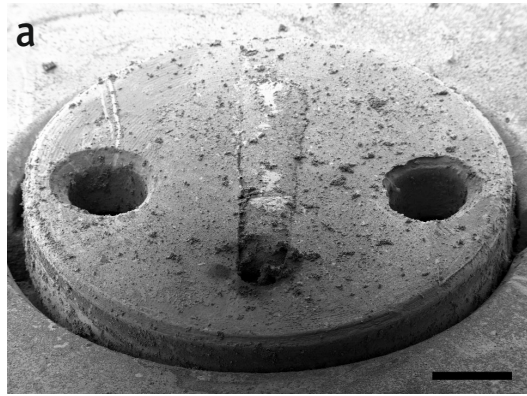
Figure 2
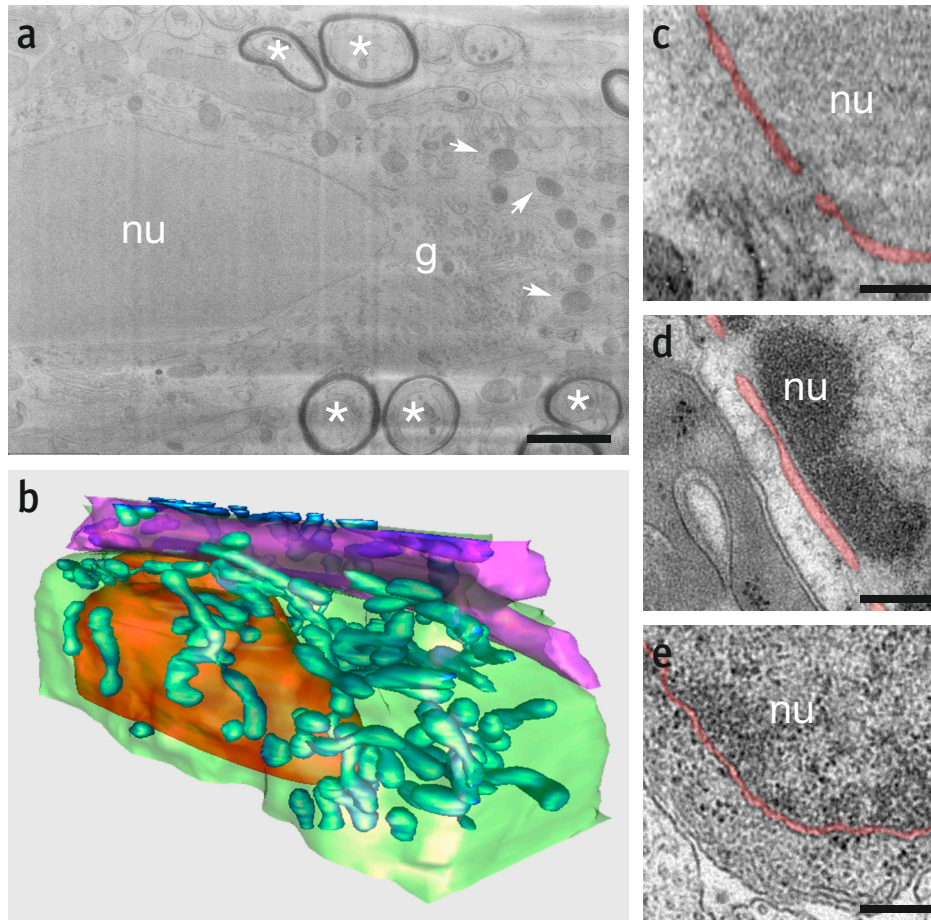
Figure 3
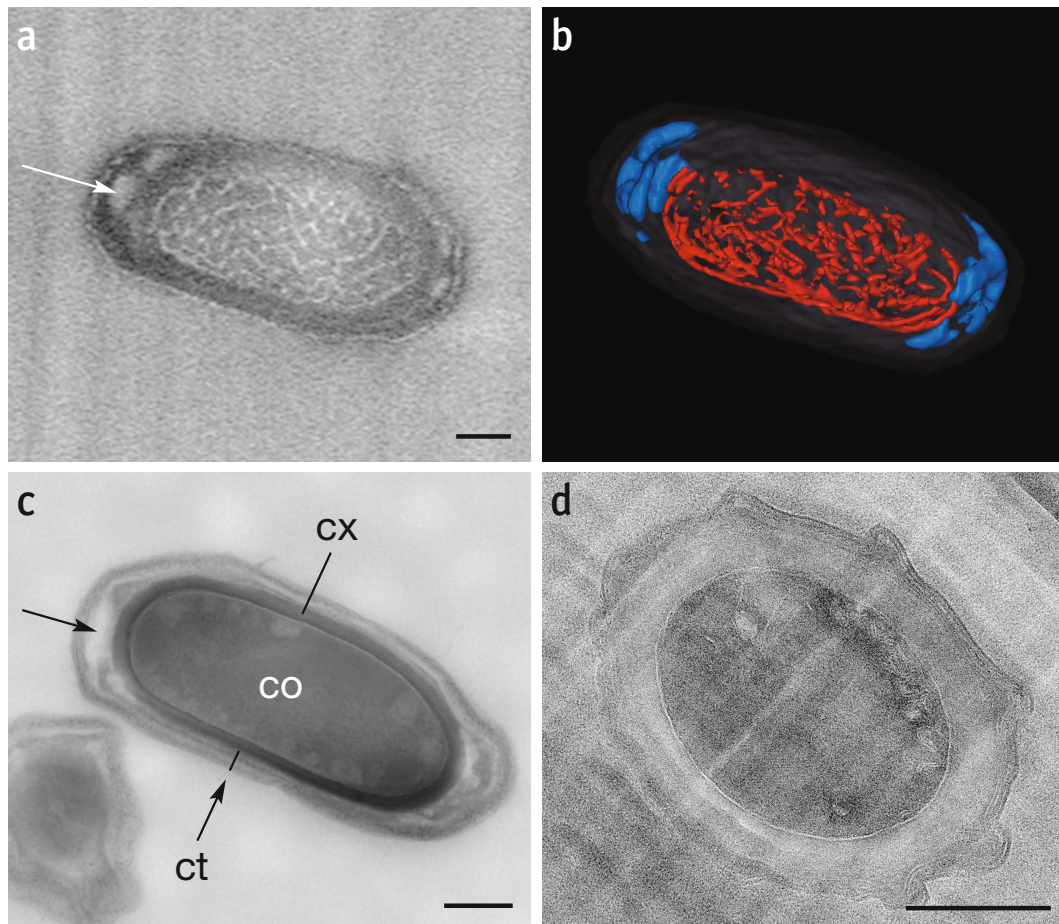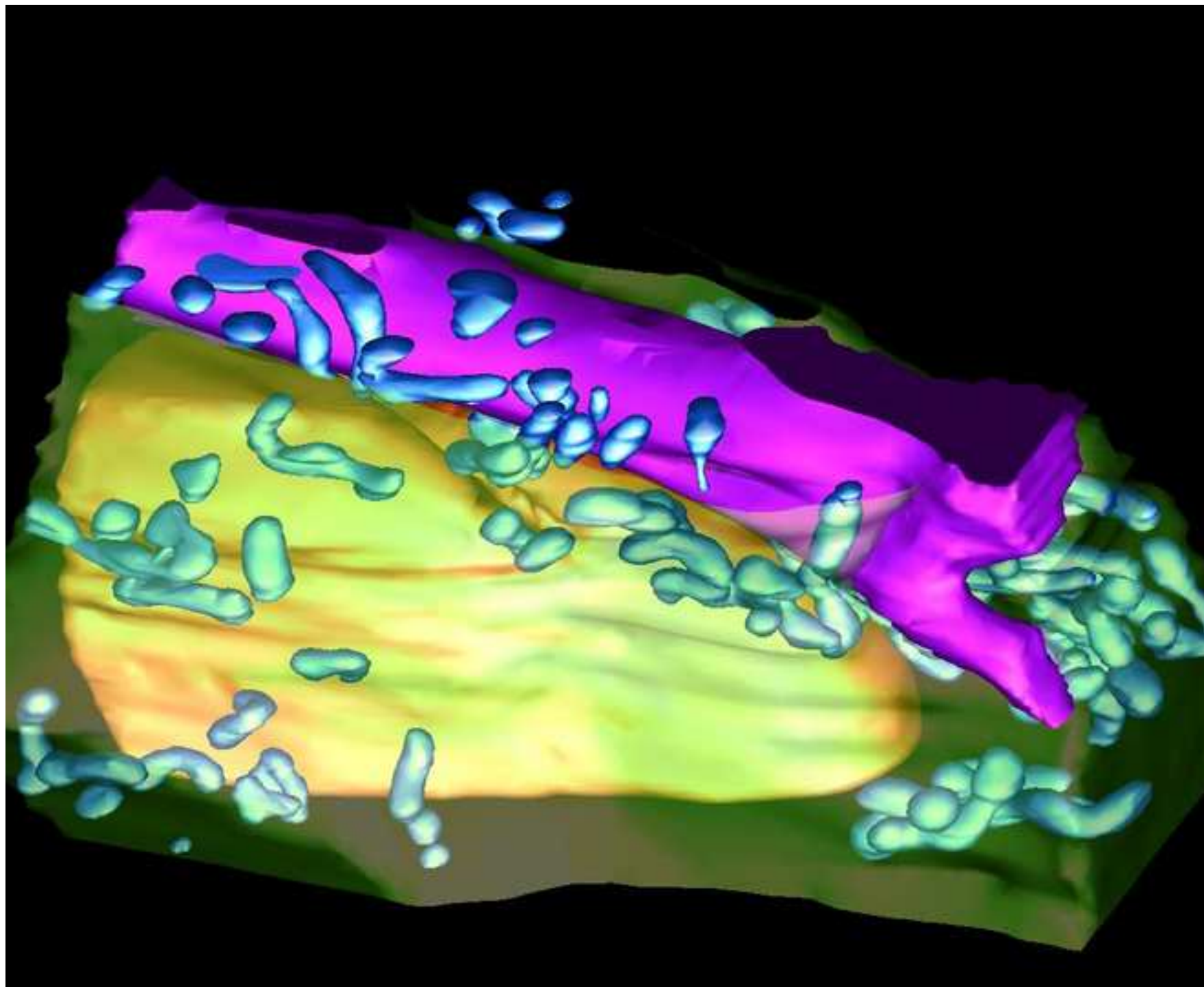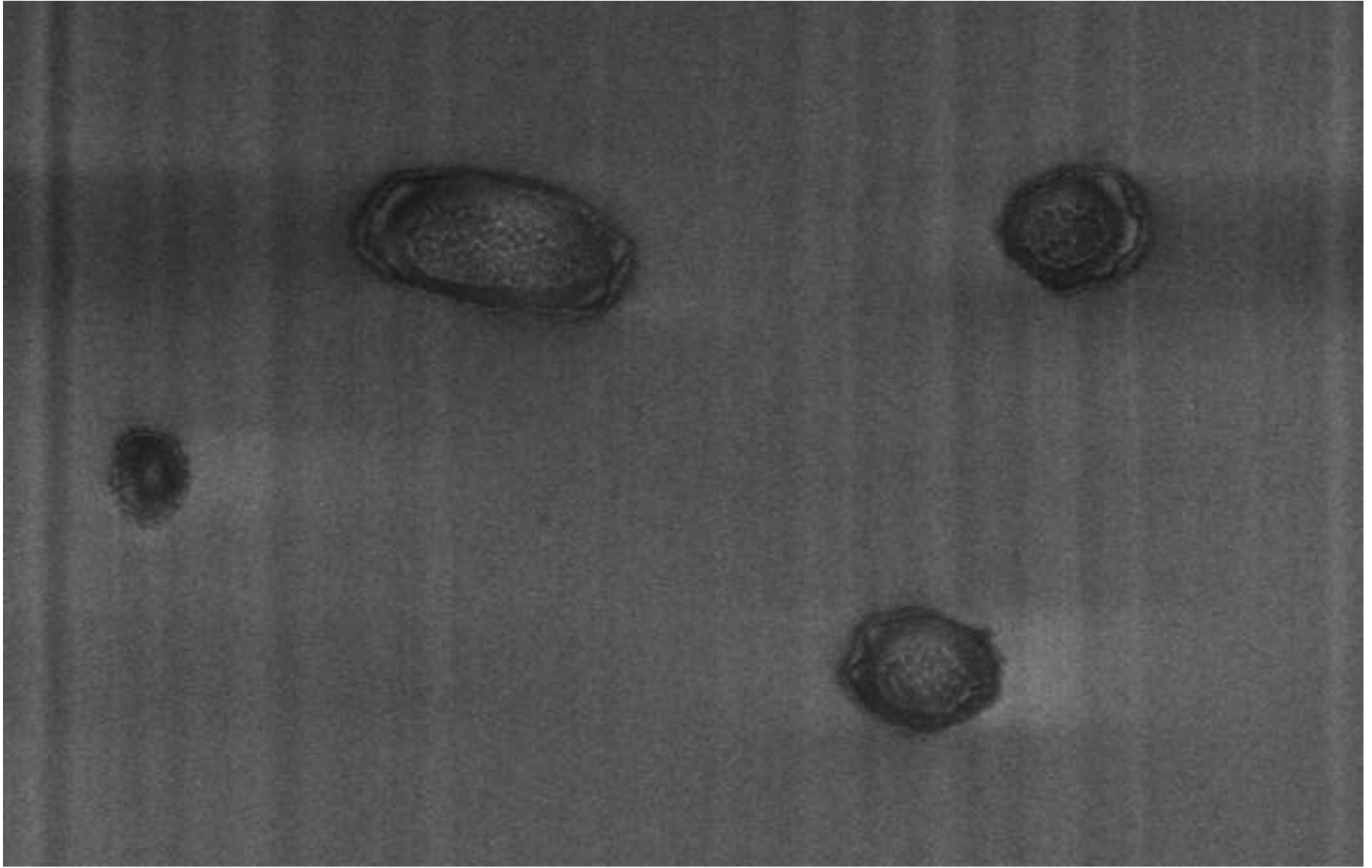
Supplementary Materials and Methods

High pressure freezing

Wildtype C57Bl6 mice at the age of 14 days were killed by cervical dislocation and the optic nerves were carefully removed and frozen by HPF in a HPM100 apparatus (Leica Microsystems, Vienna, Austria) as decribed (Möbius *et al.*, 2010) using a slit carrier and PBS containing 20 % PVP 10.000 (Sigma-Aldrich, Taufkirchen, Germany) as a cryoprotectant. Spores of *Bacillus subtilis* (ATCC 6633) were generated by using a sporulation medium based on (Sterlini and Mandelstam, 1969). They were stored in 0.05 M HEPES (pH 7.2) at a cell density of about $1 \cdot 10^9$ spores/ml in the refrigerator (5−10°C). For HPF spores were centrifuged at 4000 g for 5 min. A dense suspension was filled in 0.1 mm deep aluminum platelets, covered with a flat aluminum platelet (3 mm diameter) to form a sandwich and immediately frozen by HPF (HPF compact 01, Engineering Office M. Wohlwend GmbH).

Segmentation and 3D reconstruction

Alignment and manual segmentation on the cryo FIB-SEM image series and computation of the video of the myelinating oligodendrocyte in the mouse optic nerve was performed using IMOD (Kremer *et al.*, 1996). Segmentation and 3D visualization of spores were done by using ITK-Snap (Yushkevich *et al.*, 2006). Video clips from image series were created with ImageJ (Schneider *et al.*, 2012) (http://imagej.nih.gov/ij).

Freeze substitution and conventional processing of mouse optic nerves for TEM

After cryoimmobilization, the optic nerves were freeze substituted as described (Möbius et al., 2010). For conventional preparation, wildtype mice at the age of 14 days were killed by cervical dislocation and the optic nerves were carefully removed.

Then the nerves were fixed by immersion into a fixing solution containing 2.5 % glutaraldehyde (EM-grade, Science Services, München, Germany), 4 % formaldehyde (Serva, Heidelberg, Germany) in phosphate buffer pH 7.3 according to Karlsson and Schultz (Karlsson and Schultz, 1965) as described (Möbius et al., 2010). Ultrathin sections were placed on Formvar-coated grids (Plano, Wetzlar, Germany) and imaged in a LEO912 AB electron microscope (Carl Zeiss Microscopy GmbH, Oberkochen, Germany) with a 2k on-axis CCD camera (TRS, Moorenweis, Germany).

Assessment of perinuclear space

To estimate in a quantitative manner the width of the nuclear envelope profiles in cryo FIB-SEM images and TEM pictures of freeze substituted and conventional processed mouse optic nerves, for each condition 3 oligodendrocyte nuclei were randomly chosen and pictures of these on 10 consecutive serial sections were taken. The pictures were overlaid with a grid (300 nm^2) using ImageJ (Schneider et al., 2012) and at every second intersection the width of the nuclear envelope was determined. By this approx. 130 measurements per condition were made. The two tailed student T-test was used for calculation of significance.

CEMOVIS of Bacillus subtilis spores

Spore suspensions in PBS containing 30% dextran (approx. 40 kDa, Sigma-Aldrich, Taufkirchen, Germany) as an external cryoprotectant were taken up into copper tubes (220 µm inner and 500 µm outer diameter, Goodfellow GmbH, Bad Nauheim, Germany) as described (Han et al., 2012). A tube containing the frozen spores was fixed in a chuck in a pre-cooled (−150°C) EM FC6 cryo-ultramicrotome (Leica Microsystems, Vienna, Austria). The sample was trimmed to a rectangular shaped

block of 70–100 μm base and ca. 100 μm height, using a 20° Cryotrim-diamond knife (CT1303; Diatome, Biel, Switzerland). A 25° cryo-immuno diamond knife (Diatome, Biel, Switzerland) with a clearance angle of 6° was used to obtain ribbons of cryosections at a nominal cutting feed of 50 nm and at cutting speeds of 10 mm/s as described (Han *et al.*, 2008). Ribbons of cryo-sections were attached to pre-cooled 600 mesh EM grids with an eyelash using electrostatic charging with the Leica EM CRION (Leica Microsystems, Vienna, Austria) as described by (Pierson *et al.*, 2010). Grids with the vitreous sections were placed in a pre-cooled cryo-specimen holder (Gatan 626-DH; Gatan, Warrendale, PA, USA) and transferred into a cryo-electron microscope (JEOL JEM-1400; JEOL Germany, Eching, Germany). The accelerating voltage was set to 120 kV and the observations were performed at −178°C. The ice state in the sections was confirmed by electron diffraction. The micrographs were digitally recorded on a 4K × 4K CCD camera (F-416; TVIPS, Gauting, Germany). The electron dose on the specimen was kept between 700–1500 e^-/nm^2.

Chemical fixation and resin embedding of spores

Spores of *Bacillus subtilis* (ATCC 6633) were centrifuged and the pellet was resuspended with 2.5% glutaraldehyde in 0.05 M Hepes. After one hour of fixation at room temperature spores were dehydrated and embedded in LR White (2.5 μl accelerator per ml) on ice (Laue, 2010). Ultrathin sections were stained with mixtures of uranyl acetate and methyl cellulose (Roth *et al.*, 1990). Images were taken with a Tecnai 12 BioTwin transmission-electron microscope (FEI, Eindhoven, The Netherlands) and a 1k x 1.3k CCD camera (MegaView, OSIS) at 120 kV.

Freeze-drying of high-pressure frozen spores

Aluminum platelets with high-pressure frozen spores of *Bacillus subtilis* (ATCC 6633) were transferred into the platelet holder of a VCT100 cryo-transfer (shuttle) system (Leica Microsystems, Vienna, Austria) and inserted in a pre-cooled (−156°C) sputter coater (MED 020; Leica Microsystems, Vienna, Austria) operating at high vacuum (1·10^{-6} mbar). Temperature of the stage immediately was set to −110°C which was achieved within 10 min at 5.3·10^{-7} mbar followed by an increase to −100°C within the same time. After a dwell time of 45 min, temperature was raised in steps of 10°C from −100°C to −60°C at a rate of about 1-2°C/min (including a dwell time of about 1h at −90°C). Vacuum was constant until −80° and changed abruptly from 4.3·10^{-7} mbar to 1·10^{-6} mbar at −79°C, indicating sublimation of bulk water. Recovering of vacuum was achieved within a minute and remained constant until reaching room temperature. Finally, the stage was heated from −60° to +20° within an hour; samples were removed from the holder and stored in grid boxes.

The aluminum platelet containing the freeze-dried spores was glued to an aluminum stub using silver paint. The aluminum stub was mounted on an standard carousel holder and transferred to the Auriga60 Crossbeam® system (Carl Zeiss Microscopy GmbH, Oberkochen, Germany).

First the region of interest was protected by an electron beam induced platinum deposition using the 30 µm aperture in normal mode at 0.97 kV acceleration potential. For platinum deposition the sample was imaged in a reduced raster with 4.2 µm width and 3.3 µm height using line average with N=11 and scan speed 8 at zero degree stage tilt for 5 minutes. During the deposition process a system pressure of 1.5 ·10^{-5} mbar was measured.

A first coarse cross-sectioning was directly milled into the surface using the 30kV@600pA FIB probe current in order to achieve a viewing channel for the SEM.

For acquisition of the FIB-SEM data set the FIB probe current 30kV@50pA and a FIB slice thickness of 7 nm was used. After milling of each slice the region of interest on the block face was imaged using the 30 μm aperture in normal mode at 0.97 kV acceleration potential and the in-lens secondary electron detection. For SEM imaging the lateral pixel size was 3.5 nm and the dimensions of the imaging area were 7.16 μm in width and 5.37 μm in height (2048 pixel ·1536 pixel). For noise reduction line averaging (N=11) and a scan speed of 5 was chosen.

Supplementary References

Han, H.M., B. Zuber, J. Dubochet, 2008. Compression and crevasses in vitreous sections under different cutting conditions. J Microsc 230, 167-71.

Han, H.M., J. Huebinger, M. Grabenbauer, 2012. Self-pressurized rapid freezing (SPRF) as a simple fixation method for cryo-electron microscopy of vitreous sections. J Struct Biol 178, 84-7.

Karlsson, U., R.L. Schultz, 1965. Fixation of the Central Nervous System from Electron Microscopy by Aldehyde Perfusion. I. Preservation with Aldehyde Perfusates Versus Direct Perfusion with Osmium Tetroxide with Special Reference to Membranes and the Extracellular Space. J Ultrastruct Res 12, 160-86.

Kremer, J.R., D.N. Mastronarde, J.R. McIntosh, 1996. Computer visualization of three-dimensional image data using IMOD. J Struct Biol 116, 71-6.

Laue, M., 2010. Electron microscopy of viruses. Methods Cell Biol 96, 1-20.

Möbius, W., B. Cooper, W.A. Kaufmann, C. Imig, T. Ruhwedel, et al., 2010. Electron microscopy of the mouse central nervous system. Methods Cell Biol 96, 475-512.

Pierson, J., U. Ziese, M. Sani, P.J. Peters, 2010. Exploring vitreous cryo-section-induced compression at the macromolecular level using electron cryo-tomography; 80S yeast ribosomes appear unaffected. J Struct Biol 173, 345-9.

Roth, J., D.J. Taatjes, K.T. Tokuyasu, 1990. Contrasting of Lowicryl K4M thin sections. Histochemistry 95, 123-36.

Schneider, C.A., W.S. Rasband, K.W. Eliceiri, 2012. NIH Image to ImageJ: 25 years of image analysis. Nat Methods 9, 671-5.

Sterlini, J.M., J. Mandelstam, 1969. Commitment to sporulation in Bacillus subtilis and its relationship to development of actinomycin resistance. Biochem J 113, 29-37.

Yushkevich, P.A., J. Piven, H.C. Hazlett, R.G. Smith, S. Ho, et al., 2006. User-guided 3D active contour segmentation of anatomical structures: significantly improved efficiency and reliability. 1053-8119 31, 1116-28.

Supplementary Figure 1 –
Beam damage
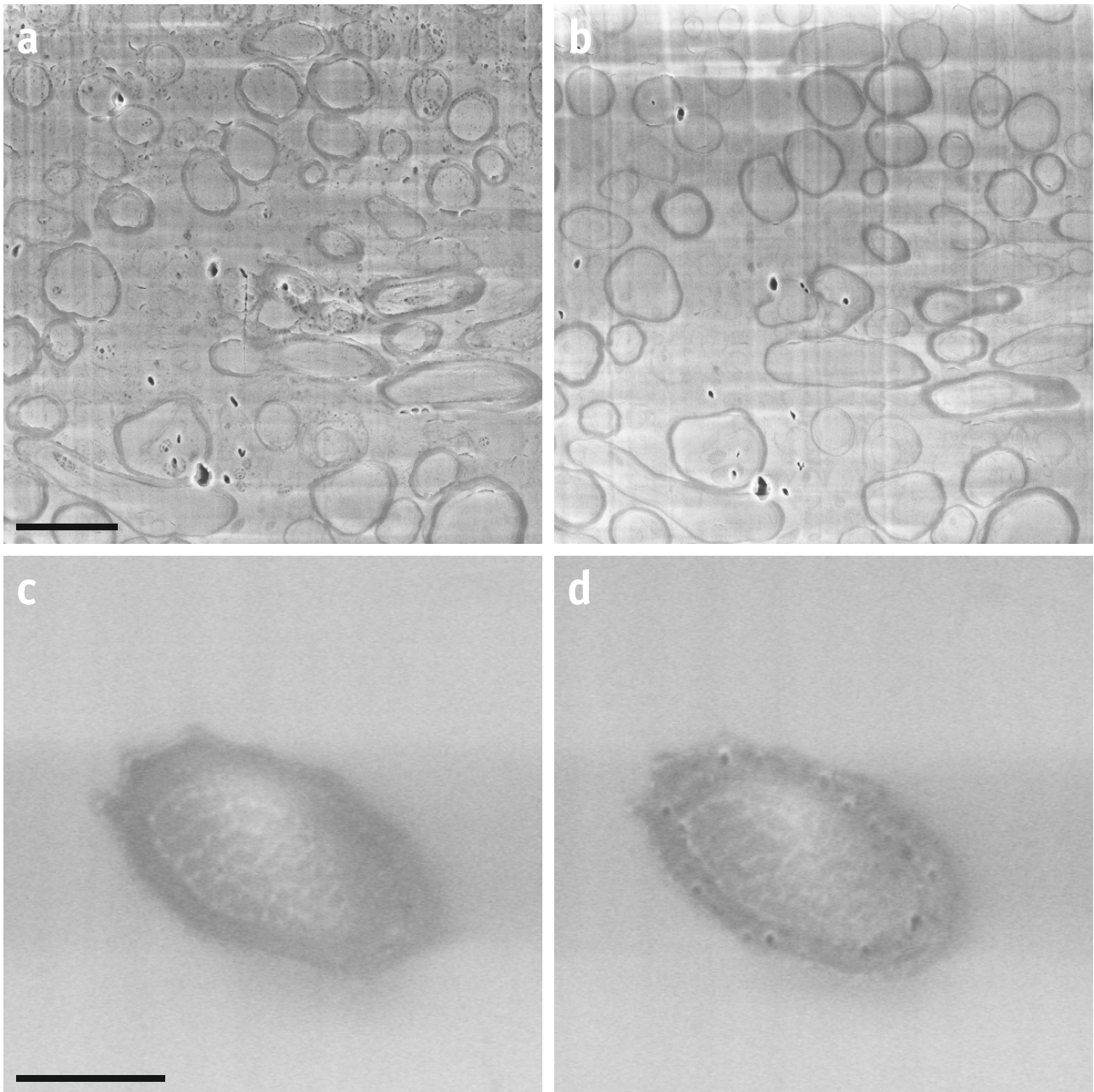
(a) Radiation damage on the frozen block face of the mouse optic nerve which happened during focussing. Prolonged radiation creates holes in the block face.

(b) The same block face after polishing with the FIB. Deep holes remain.

(c) SE-image of the block face of a dormant *Bacillus subtilis* spore.

(d) Radiation damage on the same spore, probably due to beam induced sublimation, occurs preferentially in the cortex and coat and not in the core.

Supplementary Figure 2 –
3D model of the mitochondrial network

a
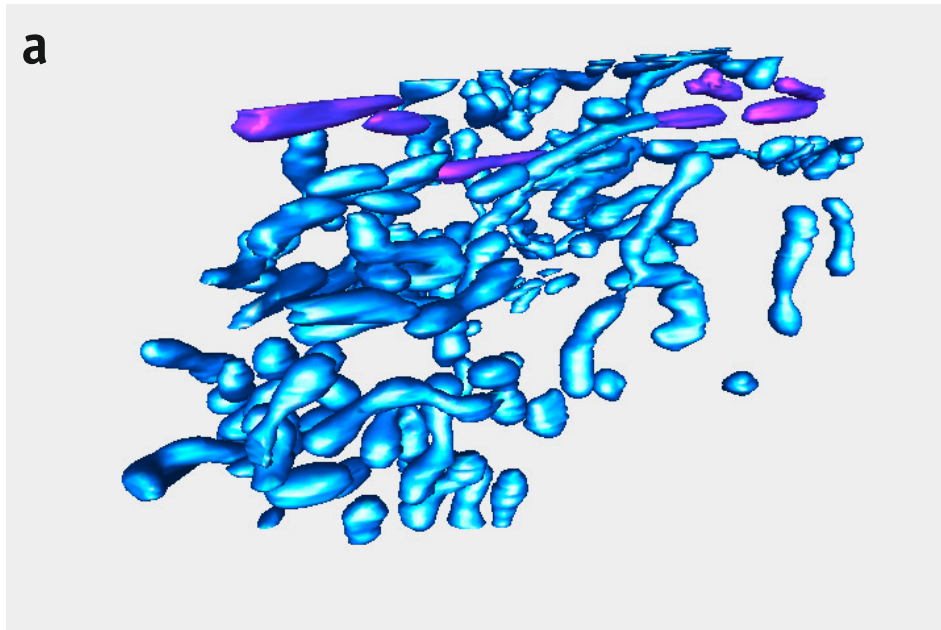
(a) 3D rendering of the mitochondria contained in the image series of the oligodendrocyte (blue) and the mitochondria in the adjacent astrocytic process (violet)

b
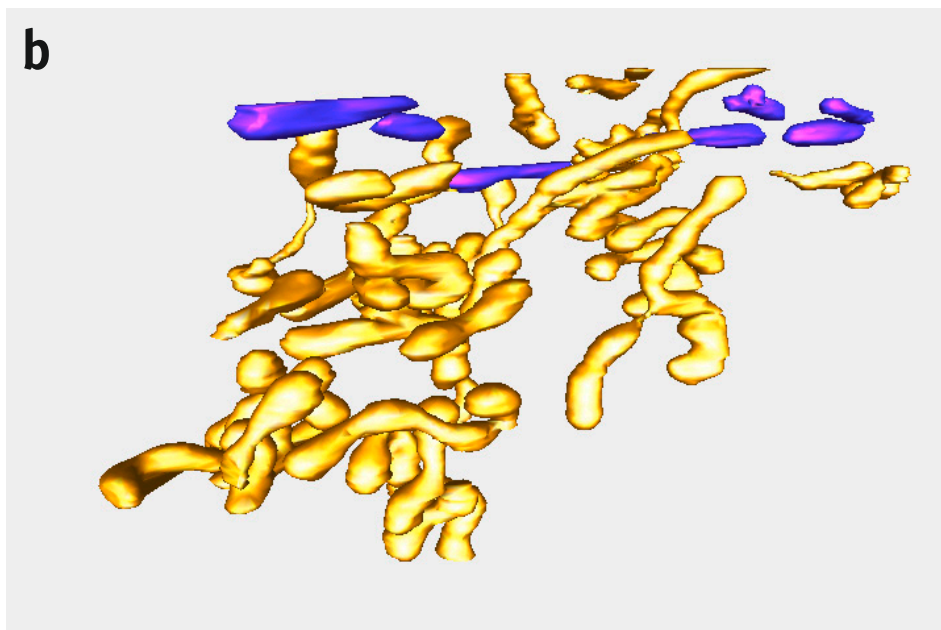
(b) Population of mitochondria which show branching and connections (yellow). The mitochondria in the astrocytic process are not branched and larger than the oligodendrocytic mitochondria.

Supplementary Figure 3 –
Influence of sample preparation on the shape of the perinuclear space
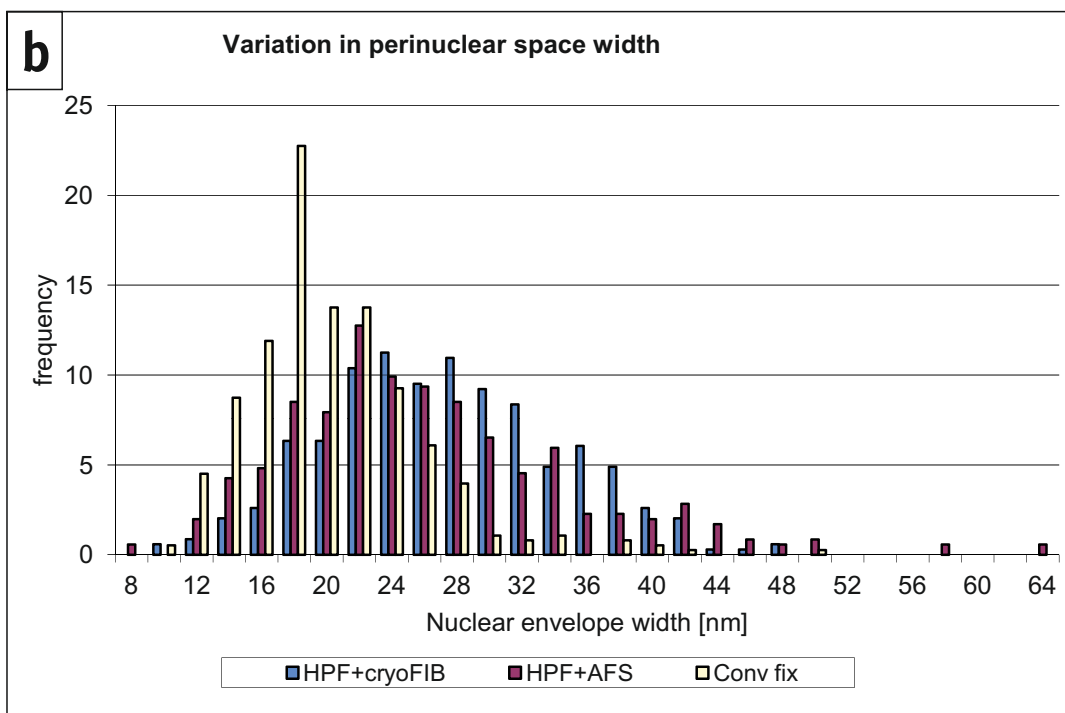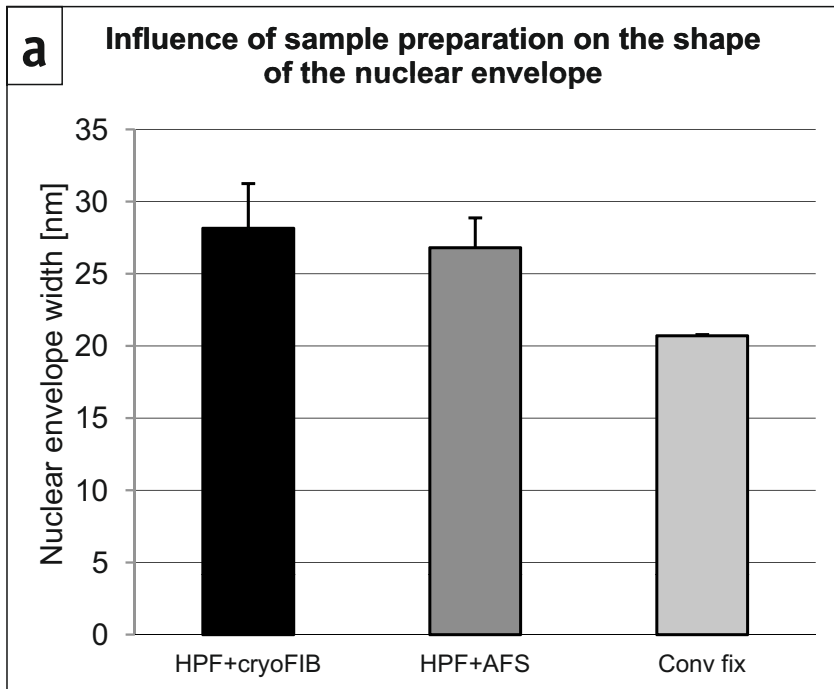
(a) The average width of the nuclear envelope profiles depending on the sample preparation method is 28.15 nm ± 3.09 SD (cryo FIB-SEM), 26.8 nm ± 2.07 SD (HPF/FS) and in conventionally prepared samples 20.7 nm ± 0.09 SD (n=3) **(b)** Variation in perinuclear space widths expressed as frequencies in the three differently prepared samples. This graph represents the fact that in cryo-prepared samples the nuclear envelope is characterized by dilated and narrow portions which may reflect biological activity. This feature is lost in the conventionally aldehyde-fixed and room-temperature embedded specimens.

Supplementary Figure 4 –
Image contrast in Bacillus subtilis spores
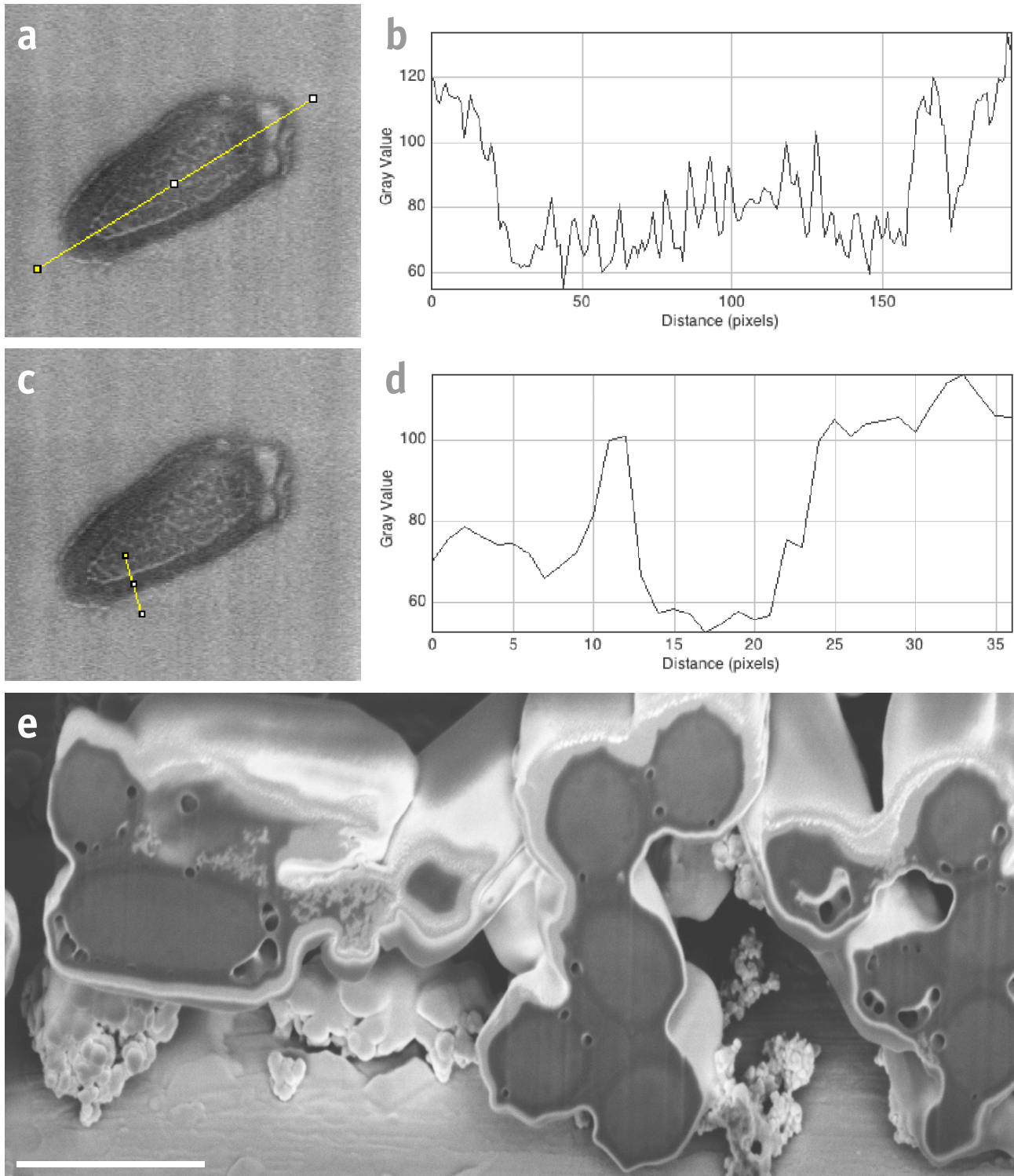
(a-b) In-Lens SE image of frozen *Bacillus subtilis* spores and brightness-plot: Similar brightness values are found for frozen water that surrounds the spore and for the cap-like structures, indicating that the bright signal is due to frozen bulk water.   (c-d) Brightness levels of the distinct outer coat layer and core structures are lower than brightness levels of the frozen bulk water present around the spore. (e) In-lens SE image of freeze-dried spores: Removal of water occurred preferentially in the cap-structure and around the spores, indicating that the highest brightness values are indeed due to structures which contain frozen bulk water.